Received: 11 August 2023 | Revised: 17 October 2023 | Accepted: 20 October 2023

DOI: 10.1002/cey2.518

RESEARCH ARTICLE

CARBON ENERGY WILEY

The effect of salt anion in ether-based electrolyte for electrochemical performance of sodium-ion batteries: A case study of hard carbon

Jiabao Li[1] | **Jingjing Hao**[1] | **Quan Yuan**[1] | **Ruoxing Wang**[1] | **Frederick Marlton**[2] | **Tianyi Wang**[1] | **Chengyin Wang**[1] | **Xin Guo**[2] | **Guoxiu Wang**[2]

[1]College of Chemistry and Chemical Engineering, Yangzhou University, Yangzhou, Jiangsu, China

[2]School of Mathematical and Physical Sciences, Centre for Clean Energy Technology, Faculty of Science, University of Technology Sydney, Sydney, Australia

Correspondence

Tianyi Wang, College of Chemistry and Chemical Engineering, Yangzhou University, 180 Si-Wang-Ting Rd, Yangzhou, Jiangsu 225002, China.
Email: wangty@yzu.edu.cn

Xin Guo and Guoxiu Wang, School of Mathematical and Physical Sciences, Centre for Clean Energy Technology, Faculty of Science, University of Technology Sydney, Sydney, Australia.
Email: xin.guo@uts.edu.au and guoxiu.wang@uts.edu.au

Funding information

Australian Research Council, Grant/Award Numbers: DP200101249, DP210101389, IH180100020; Natural Science Foundation of Jiangsu Province, Grant/Award Number: BK20210821; National Natural Science Foundation of China, Grant/Award Number: 22102141

Abstract

Compared with the extensively used ester-based electrolyte, the hard carbon (HC) electrode is more compatible with the ether-based counterpart in sodium-ion batteries, which can lead to improved cycling stability and robust rate capability. However, the impact of salt anion on the electrochemical performance of HC electrodes has yet to be fully understood. In this study, the anionic chemistry in regulating the stability of electrolytes and the performance of sodium-ion batteries have been systematically investigated. This work shows discrepancies in the reductive stability of the anionic group, redox kinetics, and component/structure of solid electrolyte interface (SEI) with different salts ($NaBF_4$, $NaPF_6$, and $NaSO_3CF_3$) in the typical ether solvent (diglyme). Particularly, the density functional theory calculation manifests the preferred decomposition of PF_6^- due to the reduced reductive stability of anions in the solvation structure, thus leading to the formation of NaF-rich SEI. Further investigation on redox kinetics reveals that the $NaPF_6$/diglyme can induce the fast ionic diffusion dynamic and low charge transfer barrier for HC electrode, thus resulting in superior sodium storage performance in terms of rate capability and cycling life, which outperforms those of $NaBF_4$/diglyme and $NaSO_3CF_3$/diglyme. Importantly, this work offers valuable insights for optimizing the electrochemical behaviors of electrode materials by regulating the anionic group in the electrolyte.

KEYWORDS

ether-based electrolyte, reaction kinetics, salt anion, SEI components, sodium storage

1 | INTRODUCTION

In recent years, the rising cost of raw materials for lithium-ion batteries (LIBs) has promoted the development of alternative technologies. Sodium-ion batteries (SIBs) have shown great promise for large-scale energy storage, given the elemental abundance of sodium and the comparable energy density and manufacturing processes to LIBs.[1–3] Regarding the electrode for SIBs, hard carbon (HC) has received significant attention owing to its acceptable cost and high energy output in full cells.[4,5] The charge storage in HC can be separated into adsorption and intercalation processes, corresponding to the slope capacity above 0.1 V versus Na/Na^+ and subsequent plateau capacity below 0.1 V versus Na/Na^+, respectively.[6,7] In principle, the capacity contributions from both regions are closely associated with bulk defects, pore structure, disordered stacks, and surface chemistry of HC.[8] Additionally, serious concentration polarization at high rates results in degradation of the plateau region, leading to poor cycling and rate capability.[9] To overcome these limitations, various structure modifications, such as heteroatom doping, closed pore fabrication, ordered domain adjustment, and surface optimization, have been utilized to create a well-defined and controlled structure that enhances the sodium storage performance of the HC electrode.[10–12]

The performance of SIBs is also highly influenced by the compatibility of the electrode with the electrolyte and the properties of the associated solid electrolyte interphases (SEI).[13,14] A favorable interaction between the electrode and electrolyte results in a stable and robust SEI that can efficiently prevent the continuous decomposition of electrolytes, achieve good ionic conductivity, and contribute to high electrochemical reversibility.[15,16] Thus, a reliable electrolyte is essential to regulating the electrochemical behavior and interphase structure for high-performance SIBs with fast-charging ability, high rate capability, and robust cycling stability.[17,18] Compared with the conventional ester-based electrolytes, the ether-based electrolytes with good chemical compatibility are advantageous for the HC electrode, resulting in favorable electrode/electrolyte interaction, superior electrochemical reversibility, and the formation of robust SEI layers abundant with inorganic species.[3,8,19] Recent work by Dong et al. has demonstrated a novel co-intercalation mechanism of solvated Na^+ and Na^+ in monodispersed HC nanospheres when ether-based electrolyte was used.[5] Additionally, using an ether-based electrolyte, an ultrahigh initial Coulombic efficiency for the carbon anode has been reported by Zhang et al.[20] A uniform, thin, compact, and ionically conducting SEI layer generated in these systems plays a critical role in achieving high performance.[2,21,22] Accordingly, these inspired works have prompted extensive studies focusing on comparing the performance, mechanism, kinetics, and SEI components between ester-based electrolytes and their ether-based counterparts to achieve high-performance SIBs.

Recent studies demonstrate that the Na^+ are solvated in electrolytes, and anionic groups are arranged out of the inner solvation sheath.[23–25] In the typical sodiation process, the solvated Na^+ migrates to the electrode-electrolyte interface and undergoes desolvation, intercalation, or adsorption, corresponding to the typical charge transfer process.[26,27] Meanwhile, the solvation sheath formed by solvent and anions can be reduced to form the SEI layer during initial electrochemical cycling, and the adjustment of solvent and anion in the electrolyte is believed to be efficient for the optimization of the SEI layer.[26,28] In view of this, the anionic group occupies the outer sheath of the solvation structure, which affects the ionic migration kinetics due to steric hindrance.[24,29] Additionally, the various solvation structures, with different anionic groups, result in discrepancies in the SEI layer structure and components, which leads to electrochemical behaviors variations.[30–32] Nevertheless, the majority of studies focus on the influence of solvents in electrochemical behaviors, and less attention is paid to the effects of the anionic group on the stability of electrolyte, redox dynamics, energy barrier for charge transfer, and SEI component. Importantly, the understanding of the correlation among anionic chemistry, component/structure of the SEI layer, reaction kinetics, and electrochemical performance will facilitate rational electrolytes for building high-performance batteries.

Herein, a systematic comparison of anionic groups on the electrochemical behavior of HC in ether-based electrolytes, aiming to clarify the correlation of anionic chemistry, redox kinetics, structure/component of SEI, and electrochemical sodium storage performance, has been performed. This involved using sodium hexafluorophosphate ($NaPF_6$), sodium tetrafluoroborate ($NaBF_4$), and sodium trifluoromethanesulfonate ($NaSO_3CF_3$) as conducting salts, and diethylene glycol dimethyl ether (diglyme) as the typical ether solvent. The detailed investigation demonstrates that the preferred decomposition of PF_6^- induced an inorganic-rich SEI, satisfied ionic conductivity accompanied with high Na^+ transference number, and favorable redox kinetics of the HC electrode in $NaPF_6$/diglyme. This study shows that the HC electrode in $NaPF_6$/diglyme modifies the sodium storage performance, evidently confirming the important role of anionic chemistry in determining the electrochemical performance of the target electrode.

2 | EXPERIMENTAL SECTION

2.1 | Materials

The HC was obtained from Guangdong Canrd New Energy Technology Co., Ltd. The $NaPF_6$, $NaSO_3CF_3$, $NaBF_4$, $NaClO_4$, NaTFSI, and diglyme with battery grade were purchased from Aladdin. Note that all the slats were further dried at 80°C overnight, and the residual H_2O in the solvents employed was removed by the activated molecular sieve for 3 days.

2.2 | Electrode and electrolyte preparation

The HC, binder (sodium carboxymethyl cellulose), and conductive agent (Super P), with a mass ratio of 8:1:1, were mixed in deionized water to form a uniform slurry, and then the mixture was coated on the copper foil and further dried at 100°C overnight. Afterward, the working electrode with a diameter of 14 mm and mass loading of about 1.5 mg can be obtained after cutting. In addition, the $NaPF_6$, $NaSO_3CF_3$, $NaBF_4$, $NaClO_4$, and NaTFSI were dissolved in the diglyme to prepare the 1.0 M electrolyte. Based on the working electrode and electrolyte preparation, the coin-type (CR-2032) cells were assembled in the glovebox (oxygen content < 0.1 ppm and water content < 0.1 ppm), employing glass fiber and sodium foil as separator and counter electrode, respectively.

2.3 | Characterization

The characterizations of HC were conducted by field-emission scanning electron microscope (FESEM, Zeiss_Supra55) and X-ray diffractometer (D8 ADVANCE). The postmortem analyses of cycled electrodes, containing FESEM observation, high-resolution transmission electron microscope (HRTEM, Tecnai 12) observation, and X-ray photoelectron spectroscopy (XPS) (ESCALAB 250Xi), were carried out after washing with the diglyme. Besides, the discharge/charge measurements of HC electrodes in various electrolytes were performed on LAND 2001A. The cyclic voltammetry (CV) curves of the HC electrode in different electrolytes at various scan rates were collected from an electrochemical workstation (CHI660B), and the electrochemical impedance spectroscopy (EIS) tests were conducted on the same workstation from 10^{-2} to 10^5 Hz. The galvanostatic intermittent titration technique (GITT) tests were measured using the battery test system with a pulse current density of 0.05 A g^{-1} and a rest time of 1.0 h.

3 | RESULTS AND DISCUSSION

Taking HC as the mode electrode, a detailed investigation of electrochemical behaviors in ether-based electrolytes with various anions has been performed to determine the correlation between anionic chemistry and electrochemical behaviors. Commercial HC was employed in this study, with its corresponding FESEM and XRD pattern shown in Figure S1. As shown, the HC particles, with no special morphology, exhibit an average size of about 10–20 μm, and the typical (002) and (100) planes can be clearly detected from the diffraction pattern.[5,12] Herein, various conducting salt anions (PF_6^-, BF_4^-, $CF_3SO_3^-$, ClO_4^-, and $TFSI^-$) dispersed in diglyme were selected as the model electrolytes. In principle, the different types of anions that participated in the solvation structure are believed to induce variations in terms of electrolyte stability, redox kinetics, and sodium storage behavior. Concerning the selection of ether solvent, both liner and cyclic ether solvents, including diglyme, 1,2-dimethoxyethane, triethylene glycol monomethyl ether, and tetrahydrofuran, have been employed as solvents for SIBs.[24,25] In principle, the viscosity, compatibility with HC, dissolution ability for sodium salts, and ionic conductivity should be taken into consideration when selecting the solvent.[5,6] Particularly, the high dissolution ability for sodium salts, excellent compatibility with HC, and modest viscosity, simultaneously receiving high ionic diffusion and good chemical stability, render the diglyme to be one of the promising ether solvents for HC.[13] A detailed investigation of these effects may offer deep insights into the interaction between electrode and electrolyte.[15,33] In addition, the concentration of salt also shows a large influence on the inherent properties of electrolytes, especially for conductivity. An electrolyte with low concentration has limited charge carriers, which restricts the ion transference number, while the high viscosity in the electrolyte with high concentration impedes the ionic migration.[34,35] Thus, taking both viscosity and conductivity into consideration, the concentration of electrolyte employed in this study is 1.0 M.[3,26]

It is worth noting that the HC electrodes in electrolytes containing $NaClO_4$ and NaTFSI depict serious fluctuations upon cycling, indicating significant decomposition of electrolytes (Figure S2).[33] Accordingly, the linear sweep voltammetry (LSV) curves (Figure S3) of stainless steel|electrolyte|stainless steel cells from open-circuit voltage to 4.5 V show the discrepancy of electrochemical stability of various electrolytes, from where the oxidation current starts to rise at around 2.0 V for the

$NaClO_4$/diglyme and NaTFSI/diglyme. This demonstrates their poor antioxidation ability, and such results also reveal that the stability of diglyme-based electrolytes shows a large dependence on the anionic group employed.[36,37] Given this, the $NaClO_4$/diglyme and NaTFSI/diglyme are excluded from this study, as their limited electrochemical behavior results in the failure of the HC electrode upon charging in these electrolytes.

In principle, the correlation between anionic chemistry and electrochemical properties of electrolytes can be well built through the comparison of Na^+-diglyme and Na^+-diglyme-anion models (Figure 1A) in the lowest unoccupied molecular orbital (LUMO) and reductive stability in a single-electron reduction reaction. As shown in Figure 1B, all three models of Na^+-diglyme-PF_6^-, Na^+-diglyme-BF_4^-, and Na^+-diglyme-$CF_3SO_3^-$ demonstrate negative binding energies, thus demonstrating the high thermodynamic stability for the interaction between Na^+-diglyme and the anion.[38,39] For different salt anions, the binding energies follow the order of $CF_3SO_3^- < BF_4^- < PF_6^-$. It is reasonable to understand such binding energy order since the anions in the Na^+-diglyme-anion solvation structure primarily interact with Na^+, and the high electronegativity of F atoms in PF_6^- induces the strong interaction.[40] Noting that the relatively higher binding energy between PF_6^- and Na^+-diglyme complex allows more PF_6^- to participate in the solvation structure, which may facilitate the subsequent decomposition of anion and formation of an inorganic-rich SEI.[41]

The effect of the anionic group on the stability of electrolytes was compared through the energy level change of the LUMO of anions and diglyme after introducing an anion into a Na^+ solvation sheath.[40,41] As depicted, the LUMO energy levels of anions in solvation structure decrease, while the LUMO energy levels of diglyme increase, hence manifesting the reduced reductive stability of anions and increased reductive stability of diglyme.[38] In principle, such variation can be generally ascribed to the electron-withdrawing effect of positively charged Na^+, where the anions share the burden of the electron-withdrawing effect with the

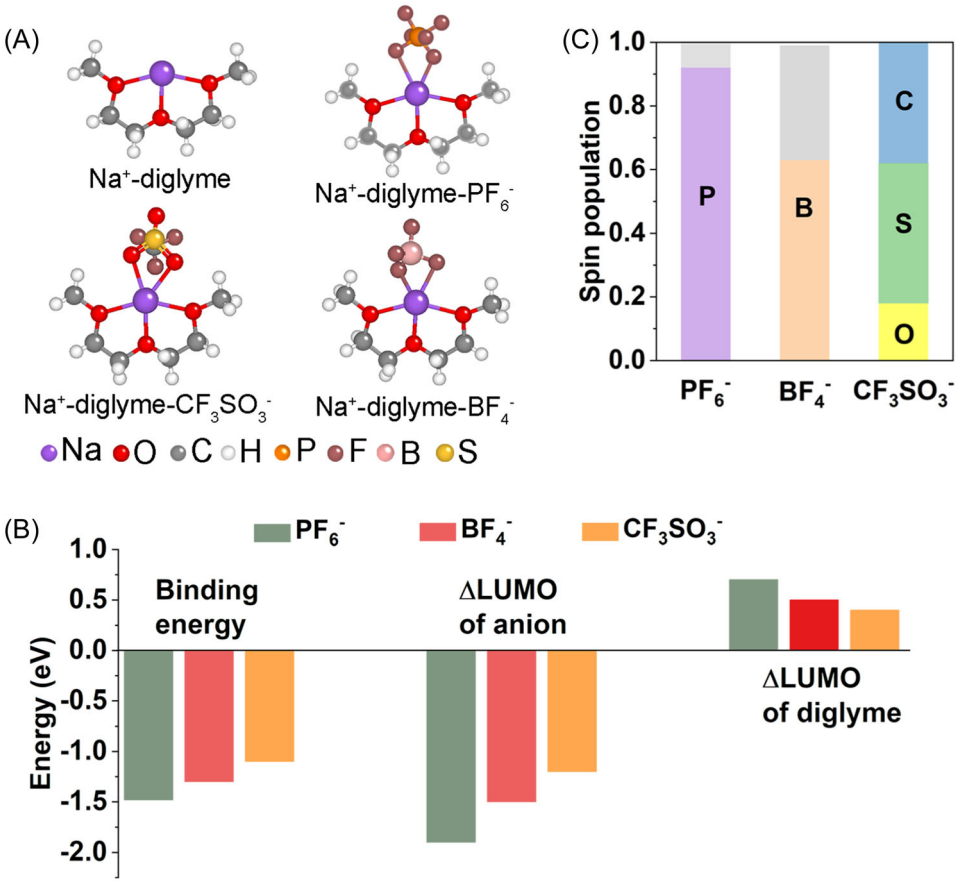

FIGURE 1 (A) Optimized geometric structures of Na^+-diglyme, Na^+-diglyme-PF_6^-, Na^+-diglyme-BF_4^-, and Na^+-diglyme-$CF_3SO_3^-$. (B) Binding energies between the Na^+-diglyme and anions as well as the energy level change of the lowest unoccupied molecular orbital of anions and solvent before and after interacting of Na^+-solvent complexes with anions. (C) Spin population values of anions in reduced Na^+-diglyme-anion complexes.

solvent, thus resulting in the reduced LUMO energy level of anions and increased LUMO energy level of diglyme.[42] Further observation of the reductive stability of anions was performed through a single-electron reduction reaction. Specifically, a single electron was added to the Na^+-diglyme-anion complexes, and the distribution of this single unpaired electron is deduced from the spin population analysis, reflecting the electron affinity of species in the Na^+ solvation sheath.[43] As seen from Figure 1C, the atoms of PF_6^-, BF_4^- and $CF_3SO_3^-$ in the solvation sheath occupy the majority of the single electron, meaning the electron aggregates around the anionic group, which in turn leads to the reduction of anions with the breaking of chemical bonds.[44] Specifically, for the $CF_3SO_3^-$, the C, S, and O atoms share the electron, while most of the electron is aggregated at around the P and B atoms of PF_6^- and BF_4^-, respectively, combined with the decreased reductive stability of the anionic group, which may result in breaking the P-F and B-F bonds, further leading to NaF-rich SEI layer.[45] Of note, the NaF-rich SEI layer is believed to provide an efficient protection layer for the target electrode and accelerate the interfacial ionic diffusion, thereby contributing to high electrochemical sodium storage performance.[27,28]

To detect the variations of structure and components of the SEI layer with different anionic groups, XPS tests for the cycled HC electrodes were carried out. The SEI layers formed in the three electrolytes show similar compositions of C, O, F, and Na (Figure S4), while the variations of peak intensities and binding energies can be observed in the corresponding high-resolution spectra. Specifically, the C 1s spectrum in $NaPF_6$/diglyme exhibits three peaks at around 284.2, 284.7, and 286.1 eV (Figure 2A), corresponding to C–C/C–H, C–O, and C═O of the organic species in SEI layer resulting from the solvent's decomposition, respectively.[10,29] The peak at 289.1 eV can be indexed to the inorganic Na_2CO_3/Na_2CO_2R. For the O 1 s spectrum in $NaPF_6$/diglyme, obvious inorganic signals of O-F and Na-O at 536.4 and 531.2 eV, respectively, can be found owing to the reduction of $NaPF_6^-$ solvent complex, while the peak at around 532.5 eV corresponds to the O–C and O–H species in SEI layer.[11] The two peaks in the F 1s spectrum can be ascribed to Na-F (683.7 eV) and the electrolyte salt (687.4 eV), and the Na-F bonds can be ascribed to the reductive decomposition of the PF_6^-.[33] Moreover, the existence of Na-F (NaF) and Na-O (Na_2O) bonds can be confirmed by the deconvoluted peaks in the Na 1 s spectrum.[15]

As shown, the C 1s, O 1s, F 1s, and Na 1s spectra for the cycled HC electrodes in $NaPF_6$/diglyme, $NaBF_4$/diglyme, and $NaSO_3CF_3$/diglyme exhibit similar fitting peaks, but the organic and inorganic species vary (Figure 2B,C). Particularly, for $NaBF_4$/diglyme and $NaSO_3CF_3$/diglyme, the SEI layer contains a higher proportion of organic species (C–C, C–H, and C–O) but a lower proportion of inorganic species (Na–F and Na–O) compared with $NaPF_6$/diglyme (Figure 2D–F). This discrepancy can be attributed to the different stability of electrolytes with various anionic groups.[46] Specifically, the comparison of inorganic/organic species in SEI layers formed in different electrolytes reveals that the SEI film generated in $NaPF_6$/diglyme features the lowest contents (27.1% and 20.9%) of organic species (C–C/C–H, and C–O), followed by $NaBF_4$/diglyme (32.5% and 24.3%) and $NaSO_3CF_3$/diglyme (36.2% and 31.8%). On the other hand, the content of Na-F in the SEI (15.2%) formed in $NaPF_6$/diglyme is higher than those of the other two electrolytes. Accordingly, it can be deduced that the preferred decomposition of PF_6^- facilitates the generation of an inorganic-rich SEI.[35] Previous studies[2,47] have proved that the inorganic species in SEI can significantly improve its ionic conductivity, thus accelerating the interfacial charge transfer and reducing the diffusion barrier, and an appropriate higher content of inorganic species will also favor better electrochemical performance by suppressing the solubility of organic sodium carbonates (such as $NaO_2CO–C_2H_4–OCO_2Na$). Moreover, the inorganic species can also result in a high Young's modulus, contributing to high mechanical strength for the SEI layer.[40] Meanwhile, an appropriate content of organic species, coupling with the inorganic species, can induce high flexibility and elasticity to accommodate for the SEI layer to accommodate the large volume expansion and resist the side reactions.[33]

Furthermore, the observation of SEI layers formed in three electrolytes through HRTEM (Figure S5) manifests that the thicknesses of SEI layers formed in $NaSO_3CF_3$/diglyme (27 nm) and $NaBF_4$/diglyme (20 nm) are slightly thicker than that of $NaPF_6$/diglyme (11 nm). This indicates that the PF_6^- in diglyme is beneficial for the generation of a thinner SEI layer, which can avoid the continuous decomposition of electrolytes.[11] In brief, the thin and inorganic-rich SEI layer, formed in $NaPF_6$/diglyme, proves the preferred decomposition of PF_6^- upon electrochemical reduction, and highlights the excellent compatibility between $NaPF_6$/diglyme and the HC electrode, thereby contributing to modifying the interfacial charge transfer kinetics.[4,48]

In addition to the obvious effect of the anionic group on the electrochemical properties of electrolytes, the ionic migration behaviors are also influenced by the anion in electrolytes. Particularly, the comparison of Nyquist plots of the prepared electrolytes at room temperature based on the steel|electrolyte|steel cells

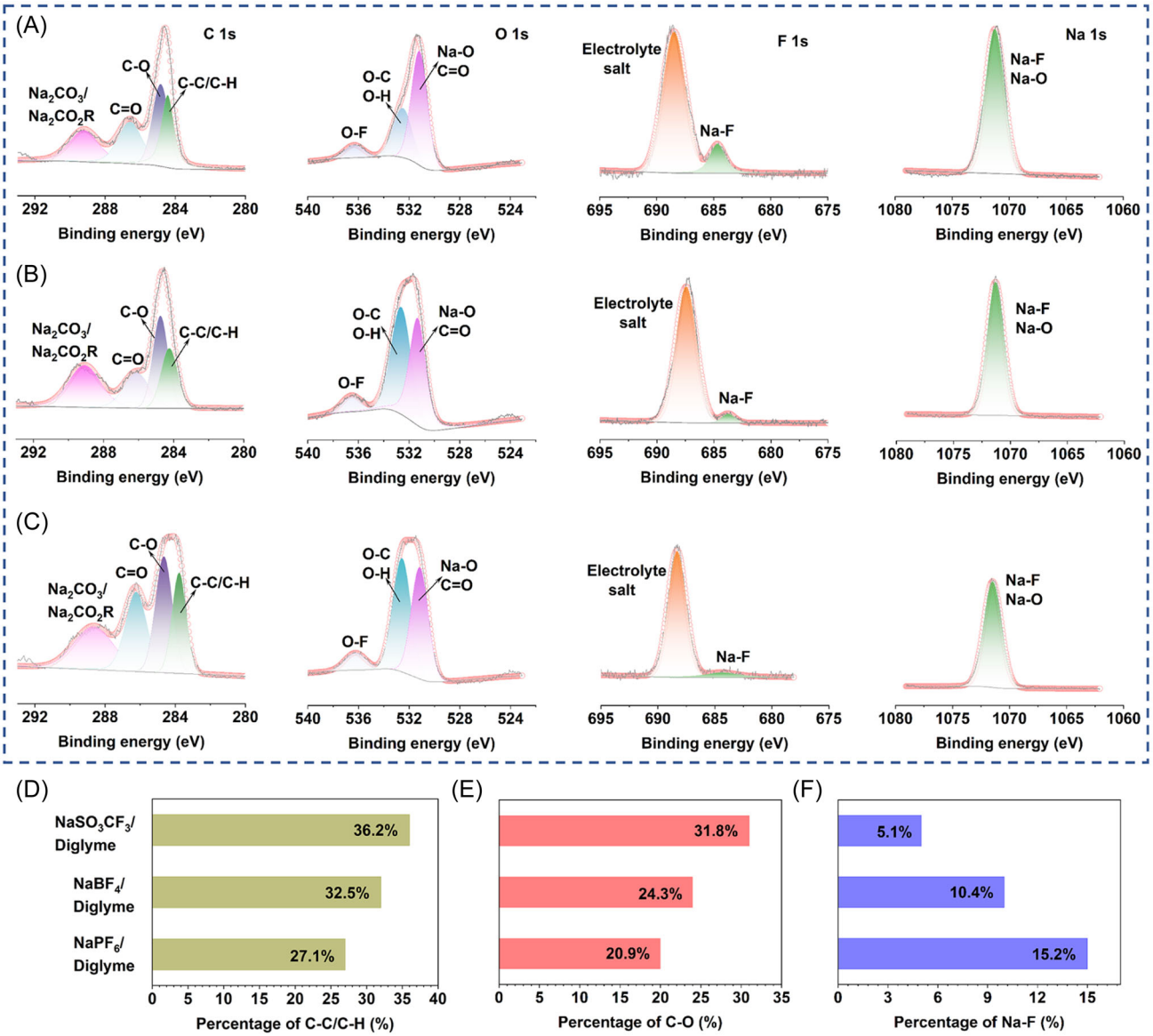

FIGURE 2 The XPS measurements for HC electrodes at 0.5 A g^{-1} after five cycles: (A) $NaPF_6$/diglyme, (B) $NaBF_4$/diglyme, and (C) $NaSO_3CF_3$/diglyme. Percentages of the (D) C–C/C–H, (E) C–O, and (F) Na–F species in the SEI layers generated on HC electrodes in three electrolytes.

reveals that the resistances of $NaPF_6$/diglyme, $NaBF_4$/diglyme, and $NaSO_3CF_3$/diglyme are, respectively, 11.9, 10.5, and 9.7 Ω, which correspond to ionic conductivities of 2.9×10^{-4}, 3.3×10^{-4}, and 3.6×10^{-4} S cm^{-1} (Figure 3A,B), according to Equation S1.[18] As known, the high binding energy between Na^+ and the anionic group may induce the formation of ion pairs and aggregates, restricting the ionic conductivity, which becomes more serious in high concentrations.[42] Nevertheless, the low concentration of 1.0 M employed in this study can guarantee the efficient dissolution of salt in diglyme, thus leading to the slight discrepancy in ionic conductivity of the three electrolytes. Except for the ionic conductivity, the anionic group also shows a large impact on the ionic transference number in the electrolyte (Equation S2). As seen from Figures 3C and S6, the Na^+ transference number of $NaPF_6$/diglyme is determined to be 0.52, much higher than those of $NaBF_4$/diglyme (0.42) and $NaSO_3CF_3$/diglyme (0.26). Combining the high binding energies between the Na^+-diglyme and PF_6^-, it can be deduced that the tight interaction of $PF_6^-$to the solvation structure impedes the migration of PF_6^-, and the restricted transference number of anionic group contributes to the high Na^+ transference number.[49] In brief, the PF_6^- in diglyme exhibits both satisfied ionic conductivity and high transference number, dramatically modifying the ionic migration and reducing concentration polarization in liquid electrolytes.

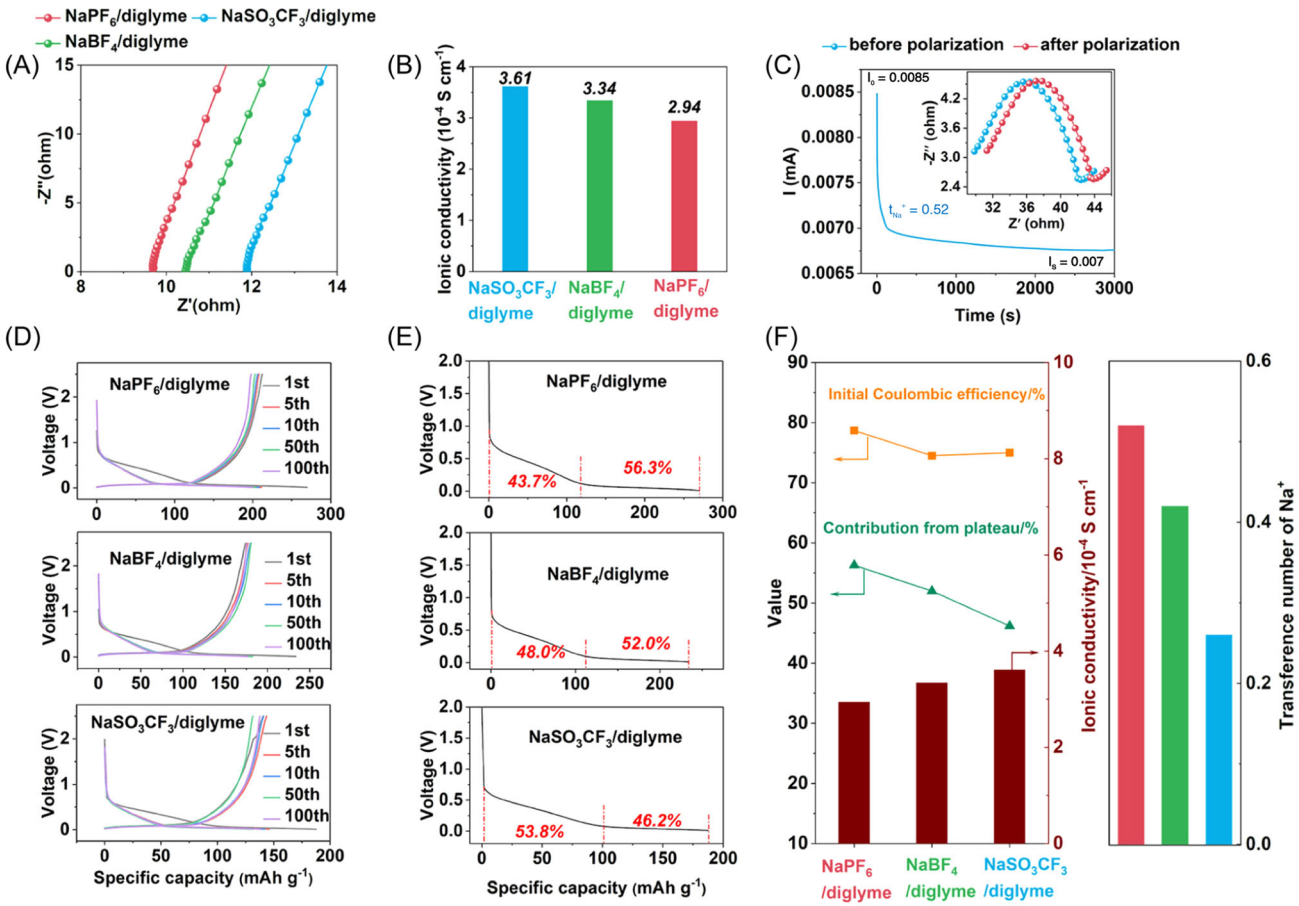

FIGURE 3 (A) Nyquist plots of three electrolytes based on steel|electrolyte|steel cells and (B) the calculated ionic conductivities. (C) Electrochemical determination of Na^+ transference number by combining a chronoamperometry experiment (DC voltage: 10 mV) with Nyquist plots (inset) for Na|electrolyte|Na cells before and after polarization in $NaPF_6$/diglyme. (D) Comparison of discharge/charge profiles at 0.5 A g^{-1}. (E) Capacity contributions from the slope and plateau of the HC electrode in three electrolytes. (F) Summary of the initial Coulombic efficiency, plateau contribution, ionic conductivity, and Na^+ transference number of HC in three electrolytes.

To detect the effect of the anionic group for a detailed understanding of sodium storage behavior, CV measurements and galvanostatic discharge/charge tests were carried out. As depicted in Figure S7, the sharp cathodic/anodic peaks at the low voltage around 0.1 V of the CV curves can be indexed to the reversible intercalation and deintercalation of Na^+, and the slight variation between the first scan and the following scans reveals good electrochemical reversibility.[48] Accordingly, the plateaus presented in discharge/charge profiles of HC in three electrolytes (Figure 3D) depict high consistency with the cathodic/anodic peaks. Specifically, the HC electrode exhibits initial discharge/charge capacities of 269.5/212.2, 233.6/174.0, and 187.6/140.7 mAh g^{-1}, acquiring initial Coulombic efficiencies of 78.7%, 74.5%, and 75.0%, in $NaPF_6$/diglyme, $NaBF_4$/diglyme, and $NaSO_3CF_3$/diglyme, respectively. In general, the preferred decomposition of PF_6^--induced stable SEI abundant with inorganic species, combined with the fats mass transport in liquid electrolyte, restricts the decomposition of electrolyte, thus improving the initial capacity of HC in $NaPF_6$/diglyme.[40] Generally, the rapid ionic migration kinetics-induced modified electrochemical reversibility accounts for the higher Coulombic efficiency of $NaPF_6$/diglyme.[50,51] Importantly, the low capacity loss upon the initial cycle of HC electrode in $NaPF_6$/diglyme manifests not only the good interaction between electrode and electrolyte but also the restricted electrolyte decomposition, resulting from the robust and inorganic-rich SEI film.[52] Except for the specific capacity, the discharge/charge profiles of the HC electrode in three electrolytes are well-maintained, hence further highlighting the good compatibility of the HC electrode with diglyme.[25]

Interestingly, detailed observation for the discharge/charge profiles demonstrates that the capacity contribution from slope and plateau varies with different anionic groups. As illustrated in Figure 3E, the capacity contributions from the plateau are calculated to be 56.3%, 52.0%, and 46.2% in

$NaPF_6$/diglyme, $NaBF_4$/diglyme, and $NaSO_3CF_3$/diglyme, respectively. In principle, the capacity from the plateau corresponds to the Na^+ intercalation, and the high capacity contribution from the plateau in $NaPF_6$/diglyme suggests convenient charge diffusion in bulk electrode, combined with the high ionic migration in liquid electrolyte mentioned above, which together guarantees rapid redox kinetics.[38,41] Accordingly, it can be concluded that the selection of anionic group not only shows an impact on the properties of electrolytes but also determines the sodium storage behaviors of the HC electrode.[53] Moreover, the schematic comparisons of initial Coulombic efficiency, plateau contribution, ionic conductivity, and Na^+ transference number in three electrolytes have been illustrated in Figure 3F, from where the superiority of $NaPF_6$/diglyme is noticeable, thus revealing the excellent compatibility between $NaPF_6$/diglyme and HC with superior ionic migration dynamics in liquid electrolyte.

The above analysis on reductive stability of electrolyte, component/structure of SEI layer, ionic migration in liquid electrolyte, and detailed sodium storage behavior has highlighted the advantage of $NaPF_6$/diglyme for HC electrode, but the investigation on the effect of anionic group for redox kinetics is insufficient. Based on the CV curves collected at various scan rates (Figures 4A and S8), the ionic diffusion kinetics in three electrolytes can be compared (Equation S3).[50] After fitting the peak current versus the square root of the scan rate, the gradient can be used to determine the ionic diffusion kinetics in bulk electrodes.[40] As illustrated (Figure 4B and Figure S8), the absolute values of the slopes for the cathodic peaks were fitted to be 0.99, 0.91, and 0.83, respectively, for $NaPF_6$/diglyme, $NaBF_4$/diglyme, and $NaSO_3CF_3$/diglyme, while the slopes for anodic peaks were 1.14, 0.55, and 0.54. This indicates that the HC electrode in $NaPF_6$/diglyme features faster ionic diffusion kinetics than those in $NaBF_4$/diglyme and $NaSO_3CF_3$/diglyme, which is attributed to the high ionic migration in electrolyte and robust SEI layer abundant with inorganic species.[16] Further detailed comparison of ionic diffusion coefficients in three electrolytes through galvanostatic intermittent titration technology (Figures 4C and S9) depicts that the excellent compatibility between $NaPF_6$/diglyme and HC induces rapid Na^+ diffusion, showing higher average Na^+ diffusion coefficients than those of $NaBF_4$/diglyme and $NaSO_3CF_3$/diglyme. Noting that the coefficients at the plateau region are relatively lower compared with the slope region, thus demonstrating that the interaction is controlled by the diffusion behavior, and the high ionic dynamics of HC in $NaPF_6$/diglyme can facilitate the charge transportation, resulting in modified electrochemical sodium storage performance.[30,39]

As demonstrated above, the $NaPF_6$/diglyme can induce the generation of an inorganic-rich SEI, hence

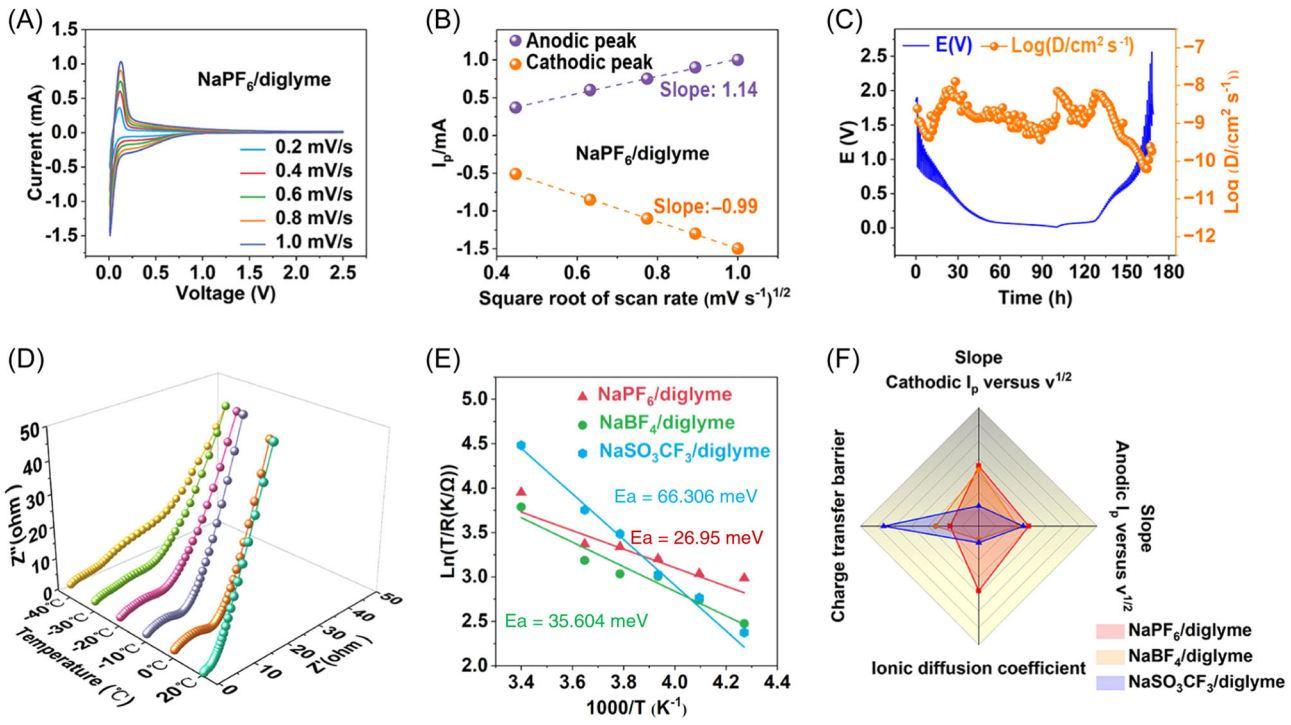

FIGURE 4 (A) CV curves with different scan rates, (B) fitted lines of peak current versus square root of scan rate, (C) GITT curves and calculated Na^+ diffusion coefficients, (D) Nyquist plots at various temperatures, and (E) Arrhenius plots of HC electrode in $NaPF_6$/diglyme. (F) Comparison of kinetics parameters of HC electrodes in three electrolytes.

reducing the charge-transfer barrier and promoting redox kinetics.[54] To verify this view, the EIS spectrum of HC electrodes under various temperatures in different electrolytes and corresponding fitted Arrhenius plots have been performed. For the $NaPF_6$/diglyme (Figure 4D), Nyquist plots ranging from −40°C to 20°C illustrate that the charge transfer resistance (R_{ct}) at the middle-frequency region decreases gradually with an increase in temperature. This trend can be also found for $NaBF_4$/diglyme and $NaSO_3CF_3$/diglyme (Figure S10). The Arrhenius plots (Figure 4E) obtained according to Equation S4 manifest that the energy barriers for charge transfer in $NaPF_6$/diglyme, $NaBF_4$/diglyme, and $NaSO_3CF_3$/diglyme are fitted to be 26.95, 35.60, and 66.31 meV, respectively.[29] Generally, it is believed that the inherent high ionic migration kinetics in both electrolyte and electrode and robust SEI layer abundant with inorganic species contributes to the low energy barrier of charge transfer in $NaPF_6$/diglyme, which in turn facilitates the redox reaction and improves the battery performance.[38] Also, the comparison of kinetics parameters in three electrolytes has been schematically illustrated in Figure 4F, from where the $NaPF_6$/diglyme exhibits superiority in both ionic diffusion and charge transfer barrier. Further combined with the high Na^+ transference number and satisfied ionic conductivity in the liquid electrolyte, excellent sodium storage performance is deemed to be obtained.[24]

As depicted above, the superior compatibility between the HC electrode and $NaPF_6$/diglyme is evident from the characterizations and electrochemical measurements, where the high ionic migration in liquid electrolyte, rapid ionic diffusion in bulk electrode, and robust inorganic-rich SEI layer is believed to boost the sodium storage performance of the HC electrode. Figure 5A illustrates the cycling performance of the HC electrode in $NaPF_6$/diglyme, $NaBF_4$/diglyme, and $NaSO_3CF_3$/diglyme at 0.5 A g^{-1}. Obviously, the HC in $NaPF_6$/diglyme displays higher specific capacity and better cycling stability than those of $NaBF_4$/diglyme and $NaSO_3CF_3$/diglyme. Particularly, after 100 cycles, the reversible capacities of the HC electrode in $NaPF_6$/diglyme, $NaBF_4$/diglyme, and $NaSO_3CF_3$/diglyme at 0.5 A g^{-1} are 198.8, 175.9, and 138.1 mAh g^{-1}, respectively. Besides, the HC electrode in $NaPF_6$/diglyme exhibits higher and more stable Coulombic efficiencies compared with those in $NaBF_4$/diglyme and $NaSO_3CF_3$/diglyme (Figure 5B). Regarding the rate capability (Figure 5C), the HC electrode in $NaPF_6$/diglyme also outperforms the ones in $NaBF_4$/diglyme and $NaSO_3CF_3$/diglyme in terms of the specific capacities at all current densities, accompanied by well-maintained Coulombic efficiencies (Figure S11). Specifically, the HC electrode in $NaPF_6$/diglyme exhibits reversible capacities of 206.5, 190.1, 182.3, 172.3, and 161.2 mAh g^{-1} with current density increases of 0.5, 1.0, 2.0, 3.0, and 4.0 A g^{-1}, showing superior rate capability. Additionally, compared with the gradually degraded plateau region in $NaBF_4$/diglyme and $NaSO_3CF_3$/diglyme (Figure S12), the rate profiles of HC in $NaPF_6$/diglyme are well maintained (Figure 5D), manifesting modified electrochemical polarization, which thus results in higher specific capacities delivered by the HC electrode in $NaPF_6$/diglyme than the other electrolytes (Figure 5E).[55]

The comparison of the long-term cycling performance of HC at 4.0 A g^{-1} in three electrolytes has been shown in Figure 5F, where a higher specific capacity of 182.3 mAh g^{-1} can be obtained in $NaPF_6$/diglyme, outperforming those of $NaBF_4$/diglyme and $NaSO_3CF_3$/diglyme. Besides, the superiority of the Coulombic efficiencies of HC in $NaPF_6$/diglyme over those of $NaBF_4$/diglyme and $NaSO_3CF_3$/diglyme is shown in Figure S13. Such ultra-stable sodium storage performance can be mainly ascribed to the rapid redox kinetics, fast interfacial charge transfer, and superior interaction between electrode and electrolyte.[34] To get a deep understanding of the excellent sodium storage performance of the HC electrode in $NaPF_6$/diglyme, ex-situ Raman spectra measurements at selected voltages were performed. For the discharging, the peak intensity of the D band gradually broadens and decreases from the open circuit voltage to 1.0 V, while the peak position maintains well upon the initial discharge.[56,57] Further discharging to 0.05 V results in the left shifting of the G band and the disappearance of the D band, thus confirming the intercalation of sodium ions into the carbon layers and filling of nanopores.[58] Regarding the reverse charging, the G band shows a gradual shift toward the right, and the D band appears again with the process of charging depth.[56] In brief, the reversible variations of G and D bands of HC in $NaPF_6$/diglyme demonstrate that the excellent electrode/electrolyte interaction induces excellent electrochemical reversibility, thus contributing to stable cycling and high energy output.

To further understand the inherent effect of salt anion on the compatibility between electrode and electrolyte, FESEM investigations on the HC electrode after cycling in three electrolytes were conducted (Figure 6A–F). After 50 and 100 cycles, the corrosion of electrolytes to the electrode is evident for all three electrolytes. Even so, the HC particles can still be observed for the $NaPF_6$/diglyme, while no HC can be detected in $NaBF_4$/diglyme and $NaSO_3CF_3$/diglyme, revealing good compatibility between HC and $NaPF_6$/diglyme. Compared with the smooth surface of the HC electrode in $NaPF_6$/diglyme, the surfaces of the HC

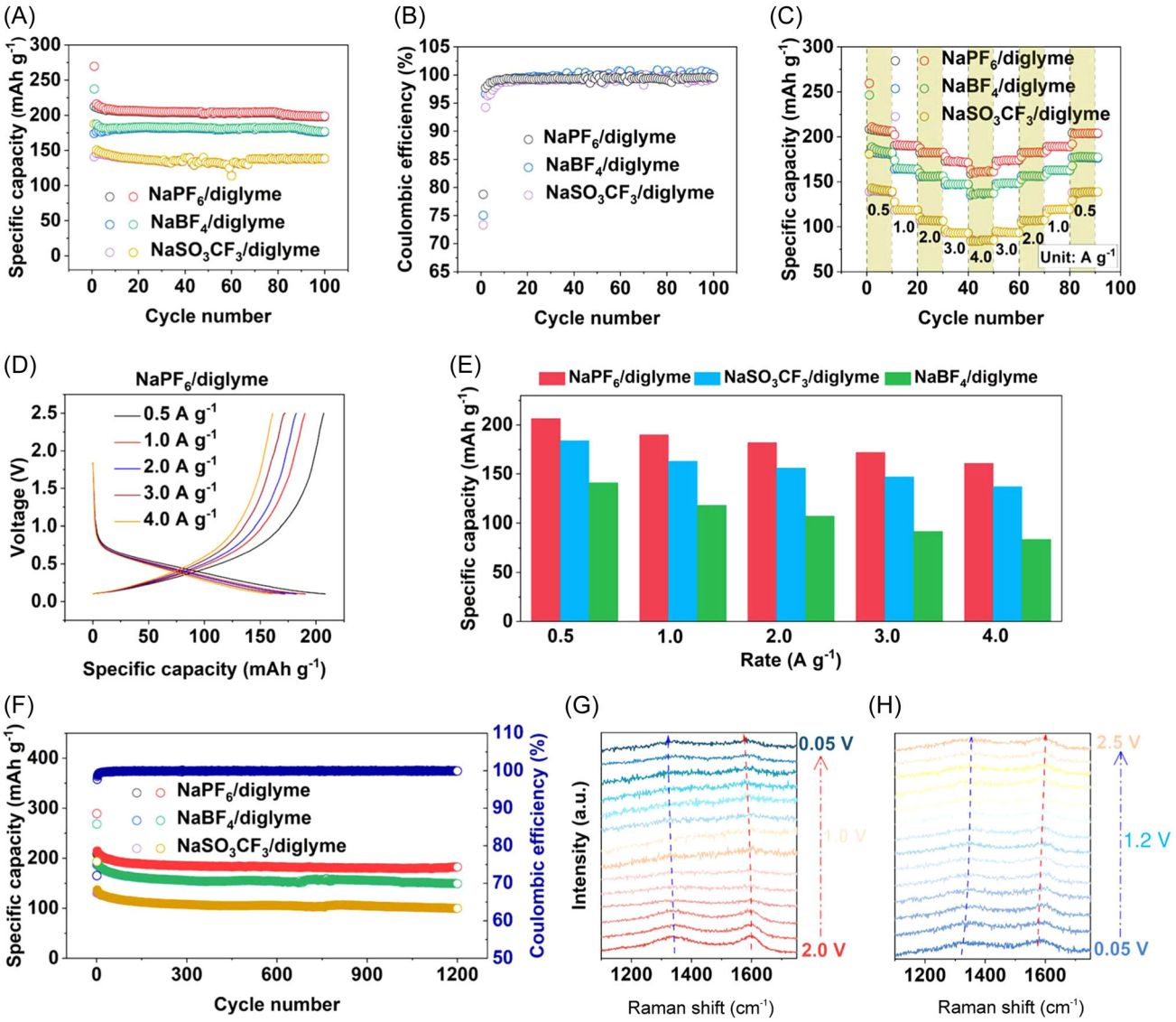

FIGURE 5 The comparison of sodium storage performance of HC electrode in three electrolytes: (A) cycling at 0.5 A g^{-1}, (B) Coulombic efficiencies, and (C) rate capability. (D) Rate profiles of HC electrode in $NaPF_6$/diglyme. (E) Comparison of rate capabilities of HC in three electrolytes. (F) Long-term cycling of HC electrode in $NaPF_6$/diglyme at 4.0 A g^{-1}. Ex-situ Raman spectra of HC in $NaPF_6$/diglyme upon (G) discharge and (H) charge.

electrode in $NaBF_4$/diglyme and $NaSO_3CF_3$/diglyme become much rougher, which may increase the ionic diffusion length and cause increased electrochemical polarization.[57] As known, the charge transfer resistance (R_{ct}) is a typical index to estimate the interfacial kinetics, and the comparison of R_{ct} for the HC electrodes in three electrolytes with different cycling numbers further reveals their discrepancies in interfacial behaviors. As illustrated in Figure 6G–I, the R_{ct} values of HC electrode in $NaPF_6$/diglyme are well-maintained and kept at relatively low values around 9.0 Ω, showing little dependence on the cycling number, which mainly results from the favorable interaction between electrode and electrolyte, rapid ionic kinetics, and stable SEI layer rich with inorganic species.[3] For the $NaBF_4$/diglyme, despite the low R_{ct} value after 10 cycles, the value gradually increases to 13 and 19 Ω after 50 and 100 cycles, respectively. In regard to the $NaSO_3CF_3$/diglyme, the R_{ct} values show a large increase with the increase of cycling number, with values of 15, 78, and 138 Ω, after 10, 50, and 100 cycles, respectively. The gradual increase in R_{ct} of HC electrode in $NaSO_3CF_3$/diglyme is attributed to the high energy barrier at the interface for charge transfer, restricted ionic migration kinetics in liquid electrolyte and bulk electrode, and relatively thick SEI layer, which should also be responsible for its unsatisfactory electrochemical sodium storage performance.[15]

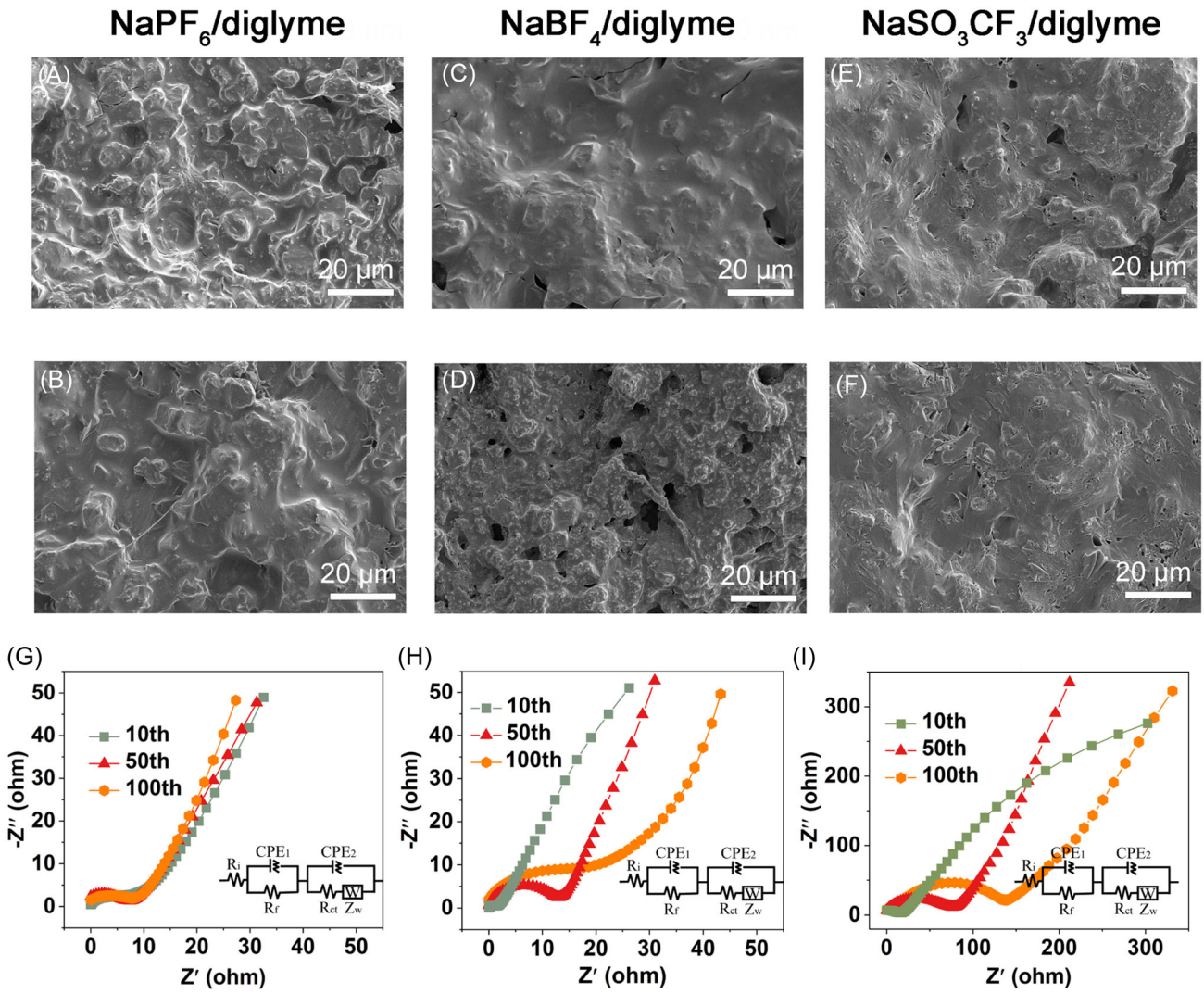

FIGURE 6 FESEM images of HC electrodes in (A, B) $NaPF_6$/diglyme, (C, D) $NaBF_4$/diglyme, and (E, F) $NaSO_3CF_3$/diglyme after 50 and 100 cycles at 0.5 A g^{-1}. Nyquist plots of HC electrode after various cycles at 0.5 A g^{-1} in (G) $NaPF_6$/diglyme, (H) $NaBF_4$/diglyme, and (I) $NaSO_3CF_3$/diglyme (the insets are the equivalent circuit models).

4 | CONCLUSION

In summary, this work presents a comprehensive study on the influence of the anionic group in diglyme for the HC electrode on the stability of the electrolyte, component/structure of the SEI layer, redox kinetics, and electrochemical sodium storage performance. The significant role of anionic chemistry in determining the properties of electrolytes and electrochemical behaviors has been clarified. Generally, the preferred decomposition of F-containing anionic group with low reductive stability will result in the generation of inorganic-rich SEI, and the excellent compatibility between the salt and solvent can induce high ionic kinetics, contributing to reducing the electrochemical polarization and modifying the electrochemical performance. Specifically, the excellent compatibility between $NaPF_6$/diglyme and HC, combined with the reduced reductive stability of PF_6^-, induces the preferred decomposition of $PF_6^-$and formation of inorganic-rich SEI, simultaneously resulting in remarkable ionic kinetics in terms of high Na^+ transference number, low energy barrier upon charge transfer, and large ionic diffusion coefficient. Accordingly, these excellent features confer the HC electrode in $NaPF_6$/diglyme with excellent sodium storage performance. More importantly, this work highlights the significance of the rational selection of salt anion in ether-based electrolytes to achieve high performance with robust rate capability and cycling stability for HC electrodes.

ACKNOWLEDGMENTS

Tianyi Wang would like to acknowledge financial support from the faculty startup funds from the Yangzhou University, the Natural Science Foundation

of Jiangsu Province (Grant No. BK20210821), the National Natural Science Foundation of China (Grant No. 22102141), and the Lvyangjinfeng Talent Program of Yangzhou. F. Marlton would like to acknowledge the support provided by the University of Technology Sydney (UTS) through the UTS Chancellor Research Fellowship. Open access publishing facilitated by University of Technology Sydney, as part of the Wiley - University of Technology Sydney agreement via the Council of Australian University Librarians.

CONFLICT OF INTEREST STATEMENT

The authors declare that there are no conflicts of interests.

ORCID

Jiabao Li http://orcid.org/0000-0001-5471-877X
Guoxiu Wang http://orcid.org/0000-0003-4295-8578

REFERENCES

1. Gao L, Chen J, Chen Q, Kong X. The chemical evolution of solid electrolyte interface in sodium metal batteries. *Sci Adv*. 2022;8(6):4606.
2. Wang C, Thenuwara AC, Luo J, et al. Extending the low-temperature operation of sodium metal batteries combining linear and cyclic ether-based electrolyte solutions. *Nat Commun*. 2022;13(1):4934.
3. Liang HJ, Gu ZY, Zhao XX, et al. Ether-based electrolyte chemistry towards high-voltage and long-life Na-ion full batteries. *Angew Chem Int Ed*. 2021;60(51):26837-26846.
4. Chen X, Liu C, Fang Y, et al. Understanding of the sodium storage mechanism in hard carbon anodes. *Carbon Energy*. 2022;4(6):1133-1150.
5. Dong R, Zheng L, Bai Y, et al. Elucidating the mechanism of fast Na storage kinetics in ether electrolytes for hard carbon anodes. *Adv Mater*. 2021;33(36):2008810.
6. Kim H, Hong J, Park YU, Kim J, Hwang I, Kang K. Sodium storage behavior in natural graphite using ether-based electrolyte systems. *Adv Funct Mater*. 2015;25(4):534-541.
7. Li X, Sun J, Zhao W, et al. Intergrowth of graphite-like crystals in hard carbon for highly reversible Na-ion storage. *Adv Funct Mater*. 2021;32(2):2106980.
8. Ma M, Cai H, Xu C, et al. Engineering solid electrolyte interface at nano-scale for high-performance hard carbon in sodium-ion batteries. *Adv Funct Mater*. 2021;31(25):2100187.
9. Sun C, Zhang X, An Y, et al. Low-temperature carbonized nitrogen-doped hard carbon nanofiber toward high-performance sodium-ion capacitors. *Energy Environ Mater*. 2023;6(4):e12603.
10. Bai P, Han X, He Y, et al. Solid electrolyte interphase manipulation towards highly stable hard carbon anodes for sodium ion batteries. *Energy Storage Mater*. 2020;25:324-333.
11. Hirsh HS, Sayahpour B, Shen A, et al. Role of electrolyte in stabilizing hard carbon as an anode for rechargeable sodium-ion batteries with long cycle life. *Energy Storage Mater*. 2021;42:78-87.
12. Song M, Yi Z, Xu R, et al. Towards enhanced sodium storage of hard carbon anodes: regulating the oxygen content in precursor by low-temperature hydrogen reduction. *Energy Storage Mater*. 2022;51:620-629.
13. Tao L, Sittisomwong P, Ma B, et al. Tailoring solid-electrolyte interphase and solvation structure for subzero temperature, fast-charging, and long-cycle-life sodium-ion batteries. *Energy Stor Mater*. 2023;55:826-835.
14. Galle Kankanamge SR, Li K, Fulfer KD, et al. Mechanism behind the unusually high conductivities of high concentrated sodium ion glyme-based electrolytes. *J Phys Chem C*. 2018;122(44):25237-25246.
15. Eshetu GG, Diemant T, Hekmatfar M, et al. Impact of the electrolyte salt anion on the solid electrolyte interphase formation in sodium ion batteries. *Nano Energy*. 2019;55:327-340.
16. Zhou L, Cao Z, Zhang J, et al. Engineering sodium-ion solvation structure to stabilize sodium anodes: universal strategy for fast-charging and Safer sodium-ion batteries. *Nano Lett*. 2020;20(5):3247-3254.
17. Zhang W, Zeng F, Huang H, et al. Enhanced interphasial stability of hard carbon for sodium-ion battery via film-forming electrolyte additive. *Nano Res*. 2022;16(3):3823-3831.
18. Hu M, Ju Z, Bai Z, et al. Revealing the critical factor in metal sulfide anode performance in sodium-ion batteries: an investigation of polysulfide shuttling issues. *Small Methods*. 2019;4(1):1900673.
19. Zhang C, Wang F, Han F, et al. Improved electrochemical performance of sodium/potassium-ion batteries in ether-based electrolyte: cases study of MoS_2@C and Fe_7S_8@C anodes. *Adv Mater Interfaces*. 2020;7(13):2000486.
20. Zhang M, Li Y, Wu F, Bai Y, Wu C. Boost sodium-ion batteries to commercialization: strategies to enhance initial Coulombic efficiency of hard carbon anode. *Nano Energy*. 2021;82:105738.
21. Zhang W, Lu Y, Wan L, et al. Engineering a passivating electric double layer for high performance lithium metal batteries. *Nat Commun*. 2022;13(1):2029.
22. Gao Y, Rojas T, Wang K, et al. Low-temperature and high-rate-charging lithium metal batteries enabled by an electrochemically active monolayer-regulated interface. *Nat Energy*. 2020;5(7):534-542.
23. Yuan F, Zhang D, Li Z, et al. Unraveling the intercorrelation between micro/mesopores and K migration behavior in hard carbon. *Small*. 2022;18(12):2107113.
24. Li L, Zhao S, Hu Z, Chou SL, Chen J. Developing better ester- and ether-based electrolytes for potassium-ion batteries. *Chem Sci*. 2021;12(7):2345-2356.
25. Li Y, Wu F, Li Y, et al. Ether-based electrolytes for sodium ion batteries. *Chem Soc Rev*. 2022;51(11):4484-4536.
26. Tang Z, Wang H, Wu PF, et al. Electrode-electrolyte interfacial chemistry modulation for ultra-high rate sodium-ion batteries. *Angew Chem Int Ed*. 2022;61(18):202200475.
27. Wang L, Ren N, Yao Y, et al. Designing solid electrolyte interfaces towards homogeneous na deposition: theoretical guidelines for electrolyte additives and superior high-rate cycling stability. *Angew Chem Int Ed*. 2023;62(6):202214372.
28. Wang H, Zhu C, Liu J, et al. Formation of NaF-rich solid electrolyte interphase on na anode through additive-induced anion-enriched structure of Na^+ solvation. *Angew Chem Int Ed*. 2022;61(38):202208506.
29. Lv Z, Li T, Hou X, et al. Solvation structure and solid electrolyte interface engineering for excellent Na^+ storage

performances of hard carbon with the ether-based electrolytes. *Chem Eng J*. 2022;430:133143.
30. Li J, Zhuang N, Xie J, et al. K-ion storage enhancement in Sb_2O_3/reduced graphene oxide using ether-based electrolyte. *Adv Energy Mater*. 2020;10(5):1903455.
31. Goktas M, Bolli C, Buchheim J, et al. Stable and unstable diglyme-based electrolytes for batteries with sodium or graphite as electrode. *ACS Appl Mater Interfaces*. 2019;11(36):32844-32855.
32. Li X, Li J, Zhuo W, et al. In situ monitoring the potassium-ion storage enhancement in iron selenide with ether-based electrolyte. *Nano-Micro Lett*. 2021;13(1):179.
33. Fondard J, Irisarri E, Courrèges C, Palacin MR, Ponrouch A, Dedryvère R. SEI composition on hard carbon in Na-ion batteries after long cycling: influence of salts ($NaPF_6$, NaTFSI) and additives (FEC, DMCF). *J Electrochem Soc*. 2020;167(7):070526.
34. Jiang R, Hong L, Liu Y, et al. An acetamide additive stabilizing ultra-low concentration electrolyte for long-cycling and high-rate sodium metal battery. *Energy Stor Mater*. 2021;42:370-379.
35. Chen C, Wu M, Liu J, Xu Z, Zaghib K, Wang Y. Effects of ester-based electrolyte composition and salt concentration on the Na-storage stability of hard carbon anodes. *J Power Sources*. 2020;471:228455.
36. Xie J, Li X, Lai H, et al. A robust solid electrolyte interphase layer augments the ion storage capacity of bimetallic-sulfide-containing potassium-ion batteries. *Angew Chem Int Ed*. 2019;58(41):14740-14747.
37. Ji Y, Sun H, Li Z, et al. Salt engineering toward stable cation migration of Na metal anodes. *J Mater Chem A*. 2022;10(48):25539-25545.
38. Yao N, Sun SY, Chen X, et al. The anionic chemistry in regulating the reductive stability of electrolytes for lithium metal batteries. *Angew Chem Int Ed*. 2022;61(52):202210859.
39. Zhou L, Cao Z, Wahyudi W, et al. Electrolyte engineering enables high stability and capacity alloying anodes for sodium and potassium ion batteries. *ACS Energy Lett*. 2020;5(3):766-776.
40. Chen X, Zhang XQ, Li HR, Zhang Q. Cation-solvent, cation-anion, and solvent-solvent interactions with electrolyte solvation in lithium batteries. *Batteries Supercaps*. 2019;2(2):128-131.
41. Yao N, Chen X, Shen X, et al. An atomic insight into the chemical origin and variation of the dielectric constant in liquid electrolytes. *Angew Chem Int Ed*. 2021;60(39):21473-21478.
42. Zhang S, Yang G, Liu Z, et al. Competitive solvation enhanced stability of lithium metal anode in dual-salt electrolyte. *Nano Lett*. 2021;21(7):3310-3317.
43. Chen J, Fan X, Li Q, et al. Electrolyte design for LiF-rich solid-electrolyte interfaces to enable high-performance microsized alloy anodes for batteries. *Nat Energy*. 2020;5(5):386-397.
44. Li J, Hu Y, Xie H, et al. Weak cation-solvent interactions in ether-based electrolytes stabilizing potassium-ion batteries. *Angew Chem Int Ed*. 2022;61(33):202208291.
45. Ould DMC, Menkin S, Smith HE, et al. Sodium borates: expanding the electrolyte selection for sodium-ion batteries. *Angew Chem Int Ed*. 2022;61(32):202202133.
46. Yang W, Wang K, Zhou W, et al. Inspired by the Cu-driven conversion reaction: how anionic properties dictate the electrochemical performance of vanadium sulfide. *J Mater Chem A*. 2022;10(48):25575-25585.
47. Li Z, Yu R, Weng S, Zhang Q, Wang X, Guo X. Tailoring polymer electrolyte ionic conductivity for production of low-temperature operating quasi-all-solid-state lithium metal batteries. *Nat Commun*. 2023;14(1):482.
48. Le PML, Vo TD, Pan H, et al. Excellent cycling stability of sodium anode enabled by a stable solid electrolyte interphase formed in ether-based electrolytes. *Adv Funct Mater*. 2020;30(25):2001151.
49. Wu X, Chen K, Yao Z, et al. Metal organic framework reinforced polymer electrolyte with high cation transference number to enable dendrite-free solid state Li metal conversion batteries. *J Power Sources*. 2021;501:229946.
50. Li J, Li Z, Tang S, Wang T, Pan L, Wang C. Boosted electrochemical performance of $Na_3V_2(PO_4)_3$ at low temperature through synergistical F substitution and construction of interconnected nitrogen-doped carbonaceous network. *J Mater Sci Technol*. 2023;150:159-167.
51. Zhou S, Tang Z, Pan Z, et al. Regulating closed pore structure enables significantly improved sodium storage for hard carbon pyrolyzing at relatively low temperature. *SusMat*. 2022;2(3):357-367.
52. Luo C, Liu Q, Wang X, et al. Synergistic-effect of diluent to reinforce anion-solvation-derived interfacial chemistry for 4.5 V-class Li||$LiCoO_2$ batteries. *Nano Energy*. 2023;109:108323.
53. Shi J, Xu C, Lai J, et al. An amphiphilic molecule-regulated core-shell-solvation electrolyte for Li-metal batteries at ultra-low temperature. *Angew Chem*. 2023;135(13):202218151.
54. Zhang J, Li Q, Zeng Y, et al. Weakly solvating cyclic ether electrolyte for high-voltage lithium metal batteries. *ACS Energy Lett*. 2023;8(4):1752-1761.
55. Alvira D, Antorán D, Manyà JJ. Plant-derived hard carbon as anode for sodium-ion batteries: a comprehensive review to guide interdisciplinary research. *Chem Eng J*. 2022;447:137468.
56. Zhao J, He XX, Lai WH, et al. Catalytic defect-repairing using manganese ions for hard carbon anode with high-capacity and high-initial-Coulombic-efficiency in sodium-ion batteries. *Adv Energy Mater*. 2023;13(18):2300444.
57. Wang K, Sun F, Wang H, et al. Altering thermal transformation pathway to create closed pores in coal-derived hard carbon and boosting of Na^+ plateau storage for high-performance sodium-ion battery and sodium-ion capacitor. *Adv Funct Mater*. 2022;32(34):2203725.
58. Anji Reddy M, Helen M, Groß A, Fichtner M, Euchner H. Insight into sodium insertion and the storage mechanism in hard carbon. *ACS Energy Lett*. 2018;3(12):2851-2857.

SUPPORTING INFORMATION

Additional supporting information can be found online in the Supporting Information section at the end of this article.

How to cite this article: Li J, Hao J, Yuan Q, et al. The effect of salt anion in ether-based electrolyte for electrochemical performance of sodium-ion batteries: a case study of hard carbon. *Carbon Energy*. 2024;6:e518. doi:10.1002/cey2.518